Water Resources Research

RESEARCH ARTICLE
10.1029/2019WR026452

Assessment and Prediction of Pore-Scale Reactive Mixing From Experimental Conservative Transport Data

Lazaro J. Perez[1,2], Juan J. Hidalgo[1], Alexandre Puyguiraud[1], Joaquín Jiménez-Martínez[3,4], and Marco Dentz[1]

[1]Spanish National Research Council (IDAEA-CSIC), Barcelona, Spain, [2]Division of Hydrologic Sciences, Desert Research Institute, Reno, NV, USA, [3]Department Water Resources and Drinking Water, EAWAG, Dubendorf, Switzerland, [4]Department of Civil, Environmental and Geomatic Engineering, ETH Zurich, Zurich, Switzerland

Key Points:
- Reactive mixing in fluid-fluid displacement is estimated from experimental data of conservative pore-scale transport
- Hydrodynamic dispersion overestimates total mass of product at preasymptotic times
- A dispersive lamella approach upscales and predicts the reactive mixing behavior in terms of effective dispersion coefficients

Correspondence to:
M. Dentz,
marco.dentz@csic.es

Citation:
Perez, L. J., Hidalgo, J. J., Puyguiraud, A., Jiménez-Martínez, J., & Dentz, M. (2020). Assessment and prediction of pore-scale reactive mixing from experimental conservative transport data. *Water Resources Research*, *56*, e2019WR026452. https://doi.org/10.1029/2019WR026452

Received 2 OCT 2019
Accepted 15 MAY 2020
Accepted article online 25 MAY 2020

Abstract We investigate the impact of pore-scale heterogeneity on reactive mixing using experimental data from inert fluid-fluid displacement in a quasi 2-D porous medium. We interpret the invading and defending fluids as the conservative components $A + C$ and $B + C$ of the instantaneous irreversible bimolecular chemical reaction $A + B \rightarrow C$ and determine the reaction product C. We find strong growth of the reaction rate at short and intermediate times due to deformation of the mixing interface and heterogeneity-induced increase of the mixing area. This behavior is captured by a dispersive lamella approach that quantifies the mixing dynamics at the interface in terms of temporally evolving effective dispersion coefficients. The latter capture the dominant controls on the evolution of the mixing interface, namely, advective heterogeneity and transverse mixing. Reactive transport formulations based on constant hydrodynamic dispersion coefficients are not able to describe the observed behavior due to the lack of complete mixing on the support scale, which is required for these approaches to hold. These results shed some new light on the origins of heterogeneity-induced mixing and reaction dynamics in porous media and their systematic upscaling.

1. Introduction

In porous media flows, pore structure and flow heterogeneity lead to the distortion of the mixing interface between initially segregated dissolved chemical species that affects the global reactivity of the system. The resulting kinetics can be very different from the ones derived from Darcy scale Fickian theories (Dentz et al., 2011; Steefel et al., 2005) or from well-mixed reactors in the laboratory (de Anna, Dentz, et al., 2014; Gramling et al., 2002; Raje & Kapoor, 2000; Willingham et al., 2008).

Mixing is the process by which substances originally segregated into different volumes of space tend to occupy the same volume. Mixing brings reactants together, enabling them to react. Reactions are controlled by mixing if the time scale of mixing is larger than the time scale of the chemical or microbial reaction (Li et al., 2006; Simoni et al., 2005; Valocchi et al., 2019). Mixing-controlled reactions can be affected by medium heterogeneity, which enhances the system reactivity compared to reactions driven by diffusion only (Jiménez-Martínez et al., 2015; Kapoor et al., 1998; Perez et al., 2019). However, heterogeneity-induced reactions are typically overestimated at preasymptotic times by Fickian models based on hydrodynamic dispersion (de Anna, Dentz, et al., 2014; Gramling et al., 2002; Raje & Kapoor, 2000). This implies that reactants are not perfectly mixed because the concentration of the chemical species displays significant variations within a representative elementary volume (REV). Such incomplete mixing among reactants have been observed in nearly homogeneous media (Gramling et al., 2002) and heterogeneous porous media (Oates & Harvey, 2006). While an equilibrium long-time behavior of the hydrodynamic dispersion suggests that in homogeneous hydrogeological settings the impact of incomplete pore-scale mixing on the reaction rates eventually vanishes (Jose & Cirpka, 2004), the total product mass formed depends on the mixing history.

Classical reactive transport models based on the advection-dispersion-reaction equation (ADRE) assume reactants are completely mixed at the REV scale (Dentz et al., 2011). The ADRE is defined as

$$\phi \frac{\partial c_i(\mathbf{x}, t)}{\partial t} = -\nabla \cdot \left[\mathbf{q} c_i(\mathbf{x}, t) - \phi \mathbf{D} \nabla c_i(\mathbf{x}, t)\right] + r_i, \tag{1}$$

where ϕ is porosity, c_i is the concentration of reactant i, $\mathbf{q}$ is Darcy velocity, $\mathbf{D}$ is the dispersion tensor, and r_i represents the space- and time-dependent rate at which species i is produced (or removed) by the reaction. The assumption of complete mixing at the REV scale (Gramling et al., 2002; Raje & Kapoor, 2000) and the use of reaction rates r_i determined under well-mixed conditions can lead to an overestimation of reaction rates that are observed under natural conditions (Battiato et al., 2009; Dentz et al., 2011; Tartakovsky et al., 2009). Numerical (Battiato & Tartakovsky, 2011; Tartakovsky et al., 2009), laboratory (de Anna, Dentz, et al., 2014; Gramling et al., 2002; Raje & Kapoor, 2000; Willingham et al., 2008), and field studies (Davis et al., 2000; Hess et al., 2002) have shown that the complete mixing assumptions inherent to ADRE models can break down and the results incur in an overprediction of the actual reaction rate. Note that these considerations apply to the use of the ADRE based on constant average flow velocity and hydrodynamic dispersion. We assume that the pore-scale advection-diffusion reaction equation based on microscale flow and mass transfer processes fully captures the detailed mixing and reaction behavior.

Alternative approaches to model the effects of incomplete mixing on the REV scale have used mixing models based on assumed beta distributions for the REV scale concentration probability density function, time-dependent reaction rate coefficients in order to model mixing induced apparent reaction kinetics (Ginn, 2018; Sanchez-Vila et al., 2010), as well as reactive random walk and continuous time random walk models that simulate apparent reaction kinetics through reaction rules between solute particles (Ding et al., 2013; Edery et al., 2010); see also the recent review by Valocchi et al. (2019).

Recent lamella-based reactive mixing models (Bandopadhyay et al., 2017; de Anna, Dentz, et al., 2014; Le Borgne et al., 2014) take a different approach and explore the link between effective reaction rate and flow heterogeneity through the kinematics of mixing. Their primary interest lies on the characterization of mixing-limited reactions based on the deformation of the material fluid elements, called lamellae (Ranz, 1979). The lamellar representation provides a powerful approach to quantify the impact of fluid deformation on mixing (de Anna, Dentz, et al., 2014). This methodology assumes that the effective upscaled reaction rate in chemical systems is controlled by the interface length and width (de Anna, Dentz, et al., 2014; Le Borgne et al., 2014). While the stretched lamella approach provides an approximation for the mixing and reaction dynamics at early times, it does not capture the merging and overlap of lamellae due to transverse diffusion at late times (de Anna, Dentz, et al., 2014; de Anna, Jiménez-Martínez, et al., 2014). An alternative approach, termed dispersive lamella, has used the concept of effective dispersion to account for the action of flow deformation and transverse diffusion on the width of the mixing interface in Poiseuille flow (Perez et al., 2019). Similar approaches have been employed for the upscaling of reactive mixing in Darcy scale heterogeneous porous media (Cirpka & Kitanidis, 2000; Cirpka, 2002; Jose & Cirpka, 2004).

In this paper, we investigate the impact of pore-scale heterogeneity on reactive mixing based on experimental data from conservative fluid-fluid displacement (Jiménez-Martínez et al., 2015). We focus on the fast bimolecular reaction $A + B \rightarrow C$ for nonsorbing compounds with equal diffusion coefficients. This implies that diffusion is the only microscopic mixing mechanism. Furthermore, we consider fluid-fluid displacement, which macroscopically is a longitudinal mixing scenario. This reaction can be quantified in terms of conservative components. The latter are identified with the invading and defending fluids. This elementary reaction can be seen as a building block of more complex reactions. In fact, many chemical systems can be broken down to elementary reactions of the kind $A+B \rightarrow C$ (Fitts, 2002; Gutierrez-Neri et al., 2009; Matlock et al., 2001; Rolle et al., 2009, 2013). We study the impact of pore-scale flow and mass transfer mechanisms on reactive mixing in terms of the evolution of the product mass and its upscaling in terms of the longitudinal effective dispersion coefficient. This approach aims at quantifying nonstandard large-scale reaction behaviors in terms of a sound characterization of the pore-scale mixing dynamics, instead of modeling the apparent large-scale kinetics in terms of effective rate laws.

The paper is organized as follows. Section 2 describes the experimental and data analysis methodology, the upscaled dispersive lamella approach, as well as the effective dispersion concept. Section 3 discusses the evolution of the mixing interface, the evolution of the reaction efficiency, and its upscaling based on effective dispersion.

2. Methodology

We evaluate reactive mixing as quantified by the instantaneous irreversible reaction

$$A + B \rightarrow C, \tag{2}$$

which occurs at the interface between the two nonsorbing species during the displacement of B by A. All chemical species are assumed to have the same diffusion coefficient. The impact of pore-scale heterogeneity is quantified from conservative experimental data of solute transport in a quasi 2-D porous medium (Jiménez-Martínez et al., 2015). We do not consider a reactive transport experiment but derive the mixing and reaction behavior using an exact algebraic map from the conservative components which enable us to determine concentrations of the reactant and product species. This approach allows us to systematically study the heterogeneity-induced mixing and reaction behavior for an idealized reactive transport scenario.

In the following, we first summarize the experimental setup presented in Jiménez-Martínez et al. (2015), whose data we use to evaluate reactive mixing. Then we recall the approach to obtain the reactants and product concentrations from conservative components. Finally, we describe the dispersive lamella approach to upscale reactive mixing and the quantification of the effective dispersion of the mixing interface.

2.1. Experimental Data

The flow cell used in the experiments of Jiménez-Martínez et al. (2015) represents a quasi 2-D medium composed of a monolayer of randomly distributed cylindrical grains. The geometry is characterized by two length scales, the average pore throat diameter, $a = 1.07$ mm, and the average pore length $\lambda = 1.75$ mm. The porosity and absolute permeability are $\phi = 0.5$ and $\kappa = 7.5 \times 10^3$ mm^2. The medium is $L = 131$ mm long and $w = 82$ mm wide, with a thickness of 0.5 mm. We consider a window between $y = 5$ mm and $y = 77$ mm in order to avoid boundary effects. Thus, the effective width is $w = 72$ mm. The inlet consists of a two-layer triangular shape designed to prevent prior mixing of fluids before entering the medium. The experimental medium does not represent a specific geological structure but facilitates the observation of some fundamental pore-scale mass transfer and mixing behaviors.

The fluid used is a 60–40% by weight water-glycerol solution containing fluorescein, with dynamic viscosity $\eta = 3.72 \times 10^{-2}$ kg m^{-1} s^{-1} and density $\rho = 1.099 \times 10^3$ kg/m^3. Under the conditions of the experiment, fluorescein is nonsorbing. The solution containing fluorescein is injected continuously into the fluid-saturated medium. The injection is characterized by an imposed flow rate Q between the inlet and outlet boundaries of the cell using a syringe pump. The mean pore velocity is $\overline{v} = 1.7 \times 10^{-5}$ m s^{-1}. The measurement of concentrations is performed by light technique (de Anna, Dentz, et al., 2014). The model is illuminated from below with a panel light source with a spatially homogeneous intensity. An optical filter excites the fluorescent tracer, and a camera placed on top of the model captures light intensity with a resolution of 3,545 × 2,279 pixels per image. Later, the light intensity is translated to concentrations by normalizing the intensity within the pixels with the maximum intensity. The measured intensity depends linearly on the concentration over the concentration range, which makes the measurements of small concentrations much more accurate. We use Savitzky-Golay smoothing filters (Savitzky & Golay, 1964) to reduce noise in the concentration values. The Savitzky-Golay filter is preferred over standard filtering techniques because it is a simple algorithm that gives optimal results for removing noise inherent to experimental transport data (Fendorf et al., 1999).

From the average pore velocity $\overline{v}$ and the average pore length λ, we can estimate the longitudinal hydrodynamic dispersion coefficient as $D^* \sim \overline{v}\lambda \sim 10^{-8}$ m^2 s^{-1}. In fact, inspecting the evolution of the width of the mixing interface with time in section 3.1 gives the value $D^* = 1.2 \times 10^{-8}$ m^2 s^{-1}. The characteristic advection time over the pore length is defined by $\tau_v = \lambda/\overline{v} = 103$ s. The corresponding characteristic diffusion time is defined by $\tau_D = \lambda^2/2D = 5 \cdot 10^3$ s with D being the molecular diffusion coefficient. These times define the Péclet number as $Pe = \tau_D/\tau_v = 106$. The characteristic advection time from inlet to outlet is $\tau_L = L/\overline{v} = 7.71 \times 10^3$ s. Time is made dimensionless by considering pore volumes $t' = t/\tau_L$. At $t' = 1$, the initial fluid in the medium has been replaced once. For simplicity of notation, we omit the primes in the following. The flow and transport parameters are summarized in Table 1.

2.2. Conservative Components and Reactive Mixing

We use the methodology presented in Gramling et al. (2002), which is a general method to quantify fluid mixing in fast reactions in porous media. The pore-scale reactive transport problem is described by the advection-diffusion reaction equation

Table 1
Flow and Transport Parameters From the Experimental Setup of Jiménez-Martínez et al. (2015)

Parameter	Value
Flow rate ($mm^3\ s^{-1}$)	0.55
Mean velocity ($m\ s^{-1}$)	1.7×10^{-5}
Diffusion coefficient ($m^2\ s^{-1}$)	1.049×10^{-10}
Péclet number	106

$$\frac{\partial c_i(\mathbf{x},t)}{\partial t} + \mathbf{v}(\mathbf{x}) \cdot \nabla c(\mathbf{x},t) - D\nabla^2 c(\mathbf{x},t) = r_i(\mathbf{x},t), \tag{3}$$

where $\mathbf{v}(\mathbf{x})$ is the velocity field in the pore space and D the molecular diffusion coefficient. The reactant and product concentrations are denoted by $c_i(\mathbf{x},t)$ with $i = A,B,C$. The corresponding reaction rates are $r_A(\mathbf{x},t) = r_B(\mathbf{x},t) = -r(\mathbf{x},t) = -r_C(\mathbf{x},t)$. The reactants are initially segregated along an interface perpendicular to the mean flow direction at equal concentration c_0. We consider natural boundary conditions at the vertical boundaries at infinity, which is a good approximation if the mixing interface is far away from the boundaries. At the grain boundaries and the horizontal domain boundaries, zero flux conditions are specified. We consider the idealized scenario that species A and B are initially separated by a sharp interface and both species have the same initial concentration c_0. All concentrations here are normalized by c_0, which is equivalent to setting $c_0 = 1$. We define the conservative components $c_{AC}(\mathbf{x},t) = c_A(\mathbf{x},t) + c_C(\mathbf{x},t)$ and $c_{BC}(\mathbf{x},t) = c_B(\mathbf{x},t) + c_C(\mathbf{x},t)$ which satisfy the advection-diffusion equation

$$\frac{\partial c_i(\mathbf{x},t)}{\partial t} + \mathbf{v}(\mathbf{x}) \cdot \nabla c_i(\mathbf{x},t) - D\nabla^2 c_i(\mathbf{x},t) = 0, \tag{4}$$

with $i = AC, BC$. The initial conditions imply that at each position in space

$$c_{BC}(\mathbf{x},t) = 1 - c_{AC}(\mathbf{x},t). \tag{5}$$

Note that this approach is valid if, as assumed here, all reactants have the same diffusion coefficient and there is neither sorption nor mass transfer between mobile and immobile portions of the pore space.

Furthermore, we assume that the reaction between A and B is instantaneous and irreversible. This means this analysis is only valid for systems for which the mixing time is much larger than the characteristic reaction time. Under this conditions, species A and B cannot coexist at the same position $\mathbf{x}$. Thus, at a given position $\mathbf{x}$, the product concentration $c_C(\mathbf{x},t)$ equals the concentration of the minority component

$$c_C(\mathbf{x},t) = \min\left[c_{AC}(\mathbf{x},t), c_{BC}(\mathbf{x},t)\right]. \tag{6}$$

This result predicts that $c_C(\mathbf{x},t)$ is centered at the mixing interface of reactants A and B with a peak concentration of $1/2$ as the reactants and product move through the porous medium. The total mass of product $m_C(t)$ per unit thickness in the domain is obtained by integrating the concentration $c_C(\mathbf{x},t)$ over the domain

$$m_C(t) = \int d\boldsymbol{x}\ c_C(\boldsymbol{x},t). \tag{7}$$

Relations 5 and 6 are the centerpiece for mapping measured conservative concentration data onto the theoretical reactant and product concentrations. The experimental setup detailed below provides conservative transport data that is identified with the conservative component $c_{AC}(\mathbf{x},t)$. We obtain the corresponding product concentration at each point in the pore space from 6 and the reactant concentrations from

$$c_A(\mathbf{x},t) = c_{AC}(\mathbf{x},t) - \min\left[c_{AC}(\mathbf{x},t), 1 - c_{AC}(\mathbf{x},t)\right], \tag{8}$$

$$c_B(\mathbf{x},t) = 1 - c_{AC}(\mathbf{x},t) - \min\left[c_{AC}(\mathbf{x},t), 1 - c_{AC}(\mathbf{x},t)\right]. \tag{9}$$

Thus, we can evaluate the impact of pore-scale flow heterogeneity on reactive mixing by pointwise mapping of the experimental conservative transport data on the equivalent reactive transport problem.

The Fickian reference solution for the total product mass under constant flow and dispersion is (e.g., Gramling et al., 2002)

$$m_C(t) = c_0 w \phi \sqrt{\frac{4\mathcal{D}t}{\pi}}, \tag{10}$$

where w is the domain width and $\mathcal{D}$ a dispersion coefficient. Pore-scale reactive mixing in terms of the evolution of the product mass in the following is compared to this reference solution parameterized by the longitudinal hydrodynamic dispersion coefficient D^* discussed below.

2.3. Dispersive Lamella

We employ here the lamellar mixing approach developed by Perez et al. (2019) for reactive mixing in Poiseuille flow. This approach decomposes the interface into a set of partial plumes that originate from pointlike injections, which define the Green function of the pore-scale advection-diffusion problem. The dispersive lamella approach approximates the Green function based on the concept of effective dispersion as outlined in the following. Note that the stretched lamella approach (Le Borgne et al., 2015) approximates the transport Green function using a first-order expansion of the local flow field around the position of a purely advectively transported particle. The superposition of these lamellae constitutes the mixing interface.

The Green function of the pore-scale advection-diffusion problem satisfies

$$\frac{\partial g(\mathbf{x}, t|y')}{\partial t} + \mathbf{u}(\mathbf{x}) \cdot \nabla g(\mathbf{x}, t|y') - D\nabla^2 g(\mathbf{x}, t|y') = 0, \tag{11}$$

where $\mathbf{u}(\mathbf{x})$ is the pore-scale velocity field. The initial condition is $g(\mathbf{x}, t = 0|y') = \delta(x)\delta(y - y')$, in which y' is the transverse coordinate to the point source at time 0. The solution for the conservative component $c_{AC}(\mathbf{x}, t)$ can be written in terms of the Green function as

$$c_{AC}(\boldsymbol{x}, t) = c_0 \int_{\Omega_v} d\boldsymbol{x}' g(x - x', y, t|y'). \tag{12}$$

where Ω_v is the injection domain. For general spatially variable flow fields, there is no closed-form analytical solution for $g(\mathbf{x}, t)$. The lamella dispersion approach approximates this Green function based on the following reasoning. The width of the Green function grows due to diffusion and the local deformation action of the underlying flow field. Diffusive growth of the Green function transverse to the mean flow direction enables the solute to sample the medium heterogeneity, which in turn enhances its longitudinal growth and relaxes its center of mass velocity toward the mean flow velocity. These mechanisms are represented by the local effective dispersion tensor $D^e_{ij}(t|y')$ and local effective velocity $v^e_i(t|y')$, which are defined by

$$D^e_{ij}(t|y') = \frac{1}{2}\frac{d}{dt}\kappa_{ij}(t|y'), \qquad v^e_i(t|y') = \frac{d}{dt}m^{(1)}_i(t|y'). \tag{13}$$

The second central moments $\kappa_{ij}(t|y') = m^{(2)}_{ij}(t|y') - m^{(1)}_i(t)m^{(1)}_j(t|y')$ and center of mass velocity $v^e_i(t|y')$ are defined in terms of the first and second raw moments of the Green function,

$$m^{(2)}_{ij}(t|y') = \int d\boldsymbol{x}\, x_i x_j g(\boldsymbol{x}, t|y'), \qquad m^{(1)}_i(t) = \int d\boldsymbol{x}\, x_i g(\boldsymbol{x}, t|y'). \tag{14}$$

Using these definitions, we now approximate the evolution equation 11 by the following equation for the effective Green function $g^e(\mathbf{x}, t|y')$, which defines the dispersive lamella:

$$\frac{\partial g^e(\mathbf{x}, t|y')}{\partial t} + \mathbf{v}^e(t|y') \cdot \nabla g^e(\mathbf{x}, t|y') - \mathbf{D}^e(t|y')\nabla^2 g^e(\mathbf{x}, t|y') = 0. \tag{15}$$

Note that this approximation represents the Green function by a Gaussian characterized by the first and second moments (14). The effective width of the mixing interface and its growth rate are quantified by the mean second central moment and the effective dispersion coefficient

$$\kappa^e_{ij}(t) = \frac{1}{w}\int_0^w dy' \kappa^2_{ij}(t|y'), \qquad D^e_{ij}(t) = \frac{1}{w}\int_0^w dy' D^e_{ij}(t|y'). \tag{16}$$

We further approximate $\kappa_{ij}(t|y') \approx \kappa^e_{ij}(t)$ and set the off-diagonal elements to zero, $\kappa^e_{ij}(t) = 0$ for $i \neq j$. Thus, equation 15 simplifies to

$$\frac{\partial g^e(\mathbf{x}, t|y')}{\partial t} + \mathbf{v}^e(t|y') \cdot \nabla g^e(\mathbf{x}, t|y') - \mathbf{D}^e(t)\nabla^2 g^e(\mathbf{x}, t|y') = 0. \tag{17}$$

The solution of 17 factorizes into

$$g^e(\mathbf{x}, t|y') = \phi g^e_{\parallel}(x, t|y')g^e_{\perp}(y, t|y'), \tag{18}$$

where $g^e_{\parallel}(x, t|y')$ and and $g^e_{\perp}(y, t|y')$ are the Green functions in the direction of the mean flow and perpendicular to it, respectively. Note that the effective Green function does not distinguish between void and solid,

which is the reason why it is proportional to porosity. For a medium of infinite extension, both $g^e_{\parallel}(x,t|y')$ and $g^e_{\perp}(y,t|y')$ are given by Gaussians characterized by $v^e_1(t|y')$ and $D^e_{11}(t)$, and $v^e_2(t|y')$ and $D^e_{22}(t)$, respectively. Inserting the decomposition 18 into 12, we obtain

$$c_{AC}(\mathbf{x},t) = \phi c_0 \int_0^w dy' G_{AC}(x,t|y') g^e_{\perp}(y,t|y'), \tag{19}$$

where we defined

$$G_{AC}(x,t|y') = \frac{1}{2}\mathrm{erfc}\left[\frac{x - m_1(t|y')}{\sqrt{2\kappa^e_{11}(t)}}\right]. \tag{20}$$

We further simplify 19 by setting $g^e_{\perp}(y,t|y') = \delta(y-y')$, which assumes that the transverse extension of the Green function is small compared to the longitudinal. Note that the evolution of longitudinal dispersion is in fact governed by transverse diffusive mixing. In this sense, for the displacement scenario under consideration here, transverse mixing is accounted for the longitudinal profile $G_{AC}(x,t|y)$, which is characterized by effective longitudinal dispersion; see also Cirpka and Kitanidis (2000). Thus, $c_{AC}(\mathbf{x},t)$ is given by the compact expression

$$c_{AC}(\mathbf{x},t) = \phi c_0 G_{AC}(x,t|y), \tag{21}$$

where $G_{AC}(x,t|y')$ denotes the profile of the conservative component across the segment of the interface located at y'. The component profile is according to 21 obtained by summation over all segments or lamellae. The product concentration $c_C(x,t)$ is obtained from 6 and 21 as

$$c_C(x,t) = \phi c_0 \frac{1}{2}\mathrm{erfc}\left[\frac{|x - m_1(t|y)|}{\sqrt{2\sigma^2_e(t)}}\right]. \tag{22}$$

Note that this framework can in principle be used to predict the spatial distribution of the reactant and product species, which, however, is beyond the scope of the present work. The total mass produced per unit thickness is obtained by integration of 22 over space, which gives

$$m_C(t) = c_0 \phi w \sqrt{\frac{2\kappa^e_{11}(t)}{\pi}}. \tag{23}$$

Equation 23 accounts for the impact of the interface deformation and coalescence on the overall reaction rate because $\phi w \kappa_{11}(t)^{1/2}$ gives the effective area of the mixing zone. A key implication of this expression is that the mass produced by mixing in fluid-fluid displacement is proportional to the interface width $\sqrt{\kappa^e_{11}}$ in the mean flow direction. Note that the stretched lamella approach (Le Borgne et al., 2015) accounts for interface deformation through a linear approximation of the local flow velocity around the position of an advectively moving material element. As it describes independent, noninteracting segments, it does not account for transverse mixing, or coalescence of lamellae. While interface deformation leads to an increase and rapid growth of the interface length, transverse mixing leads to an increase of the width of the actual mixing interface. Both mechanisms, deformation and diffusive coalescence, are here quantified in terms of effective dispersion. Similar approaches were used on the Darcy scale to distinguish actual solute mixing from spreading (Cirpka & Kitanidis, 2000; Kitanidis, 1988; 1994) and to quantify reactive mixing (Cirpka, 2002). On the Darcy scale, effective dispersion coefficients have been determined in the framework of stochastic modeling using perturbation theory as well as numerical simulations (Beaudoin et al., 2010; Dentz et al., 2000). On the pore scale, we are not aware of any similar works along these lines. In the following section, we present how the effective width of the mixing interface is obtained from the experimental data. Note that the conceptual framework presented above is not limited to 2-D porous media but can be applied straightforwardly to 3-D media, for which the same definitions of the effective dispersion coefficients and approximations for the Green functions apply.

We want to point out here that the proposed approach focuses exclusively on dispersive mixing due to variability in the pore-scale velocity and transverse diffusion. We do not consider effects due to interphase mass-transfer processes such as sorption or trapping in low velocity zones, which were discussed in detail by Jose and Cirpka (2004).

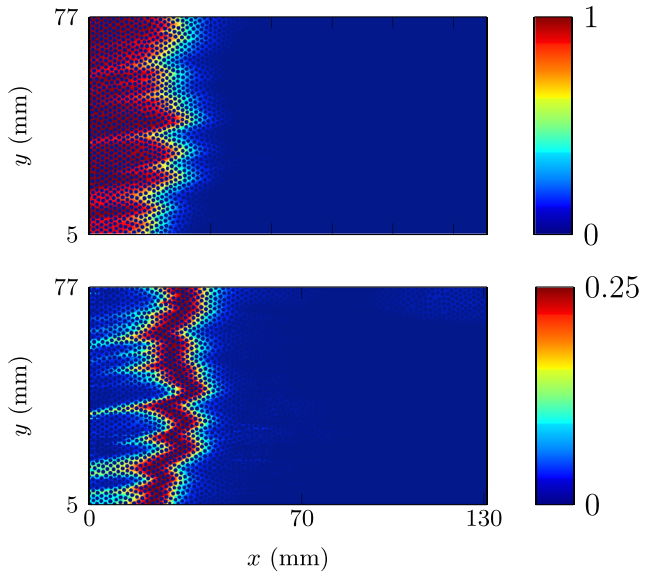

Figure 1. Map of (top) the conservative component $c_{AC}(\mathbf{x}, t)$ and (bottom) the auxiliary function $\Theta(\mathbf{x}, t)$ at $t = 0.36$ pore volume. Note that concentration are nondimensionalized by c_0.

2.4. Effective Dispersion of the Mixing Interface

In order to determine the width of the mixing interface from the data, we define the auxiliary function

$$\Theta(\mathbf{x}, t) = c_{AC}(\mathbf{x}, t)\left[1 - c_{AC}(\mathbf{x}, t)\right]. \tag{24}$$

The $\Theta(\mathbf{x}, t)$ tends to zero away from the mixing zone. This quantity is related to the segregation intensity of Danckwerts (1952). It delineates the mixing region around the interface of the advancing conservative component as shown in Figure 1. We use this approach because it can be readily determined from the experimentally available concentration map.

In order to determine the interface width, we define the ith raw horizontal moments $m_i(y, t)$ of $\Theta(\mathbf{x}, t)$ as

$$m_i(y, t) = \int dx\, x^i \Theta(\boldsymbol{x}, t). \tag{25}$$

Thus, the interface width at a vertical position y is quantified in terms of the horizontal variance

$$\sigma^2(y, t) = \frac{m_2(y, t)}{m_0(y, t)} - \frac{m_1(y, t)^2}{m_0(y, t)^2}. \tag{26}$$

The effective horizontal variance is defined by spatial averaging over the medium cross section as

$$\sigma_e^2(t) = \frac{1}{w}\int_0^w dy\, \sigma_e^2(y, t). \tag{27}$$

In the dispersive lamella approach presented in the previous section, the concentration profile across the interface is given by 20. Using 20 in 24–27 gives for $\kappa_{11}^e(t)$ in terms of $\sigma_e^2(t)$

$$\kappa_{11}^e(t) = \frac{6\sigma_e^2(t)}{5}. \tag{28}$$

We define the asymptotic effective dispersion coefficient D^* through the linear relation

$$\kappa_{11}^e(t) = \kappa_0 + 2D^* t. \tag{29}$$

Both κ_0 and D^* are obtained by fitting the data for $\kappa_{11}^e(t)$ at times $t > \tau_D$. Furthermore, we define the apparent hydrodynamic dispersion coefficient D^a as

$$D^a = \frac{\kappa_{11}^e(t_m)}{2t_m}, \tag{30}$$

where t_m is the maximum observation time.

In order to determine $\sigma_e^2(t)$ from the experimental data, we discretize the medium into horizontal layers of width Δy, for which we choose the pixel size of the image. Thus, the numerical estimator for $\sigma_e^2(t)$ is

$$\sigma_e^2(t) = \frac{1}{N_y}\sum_{k=0}^{N_y}\Delta y\sigma^2(y_k, t), \tag{31}$$

where $N_y = w/\Delta y$ and $y_k = k\Delta y$.

3. Results

In this section, we study the dynamics of predicted reactive mixing in terms of the local concentration fields of reactant A and product C and the evolution of the product mass and its quantification and upscaling in terms of the dispersive lamella approach presented above. First, we consider the evolution of the effective dispersion of the mixing interface, which is the central quantity of the dispersive lamella approach.

3.1. Evolution of the Width of the Mixing Interface

Figure 1 shows the spatial distribution of the conservative component, here interpreted as $c_{AC}(\mathbf{x}, t)$, and the interface function $\Theta(\mathbf{x}, t)$, which delineates the mixing interface. The interface is distorted due to advective heterogeneity with a width that is due to the interaction of heterogeneous advection and transverse diffusive mixing. These mechanisms are captured by the effective variance of longitudinal displacement $\kappa_{11}^e(t)$ defined in the previous section.

Figure 2 shows the temporal evolution of $\kappa_{11}^e(t)$. For times $t < \tau_v \approx 10^{-2}\tau_L$, this means when the solute has sampled less than a pore length, we expect diffusive growth. These times, however, are below the time resolution of the experiment, which is at $5 \times 10^{-2}\tau_L$ s. For times $t > \tau_v$, we observe a rapid nonlinear growth due to the interaction of interface deformation and diffusion: Lateral diffusion distributes the solute to adjacent streamlines. The velocity contrast experienced within the lamella leads then to a rapid ballistic increase of $\kappa_{11}^e(t)$. For times $t > \tau_D \approx 0.7\tau_L$, the solute has diffusively sampled velocity contrasts within a distance larger than a characteristic pore length. The velocity contrasts within the lamella are averaged out due to diffusive mixing. This explains the transition from a superlinear to the linear diffusive growth from $t > \tau_D$. In the linear regimes, we estimate the value of the asymptotic effective dispersion coefficient defined in 29 to $D^* = 1.2 \times 10^{-8}$ m^2 s^{-1}. The apparent hydrodynamic dispersion coefficient is $D^a = 1.7 \times 10^{-8}$ m^2 s^{-1}. As can be seen in Figure 2, the linear fit to the late-time data for κ_{11}^e to obtain D^* according to equation 29 leads to a large intercept κ_0. This implies that predicting longitudinal mixing with a constant dispersion coefficient D^* using a standard 1-D advection-dispersion equation must lead to an underestimation of mixing. The temporal evolution of $\kappa_{11}^e(t)$ and the asymptotic hydrodynamic dispersion coefficient D^* are used in the following to predict the reactive mixing behavior estimated from the experimental data. At late times, D^* and D^a should converge to the same value.

3.2. Dynamics of Reactive Mixing

Here we present the results for reactive mixing predicted from conservative pore-scale data using the methodology detailed in section 2.2. Figure 3 shows the distribution of the conservative component $c_{AC}(\mathbf{x}, t)$ at the two different (dimensionless) times of $t = 0.12$ and 0.77 pore volumes. The finger structure of $c_{AC}(\mathbf{x}, t)$ at early times develops due to penetration of the channels between grains, which leads to a significant increase of the length of the mixing interface (Jiménez-Martínez et al., 2015; de Anna, Jiménez-Martínez, et al., 2014). The interface is stretched by the heterogenous flow field, and a lamellar structure emerges.

As a consequence of this lamellar structure, the distribution $c_C(\mathbf{x}, t)$ of product C is heterogeneous and characterized by notable backward and forward tails. At later times, the interface homogenizes due to diffusive mixing, and we find less spatial variability in the distributions of $c_{AC}(\mathbf{x}, t)$ and $c_C(\mathbf{x}, t)$, shown in Figure 3. Advective spreading leads to a fast, ballistic initial growth of the interface length due to the velocity contrast along the interface. Transverse diffusion converts this purely advective effect into longitudinal mixing, which is captured by the effective interface width discussed in the previous section. Eventually, as the segments that form the interface mix vertically, the velocity contrast along the interface is reduced, and the ballistic growth slows down. This occurs for times larger than τ_D, at which the growth of the mixing region can be characterized by dispersive growth in terms of the constant hydrodynamic dispersion coefficient D^*.

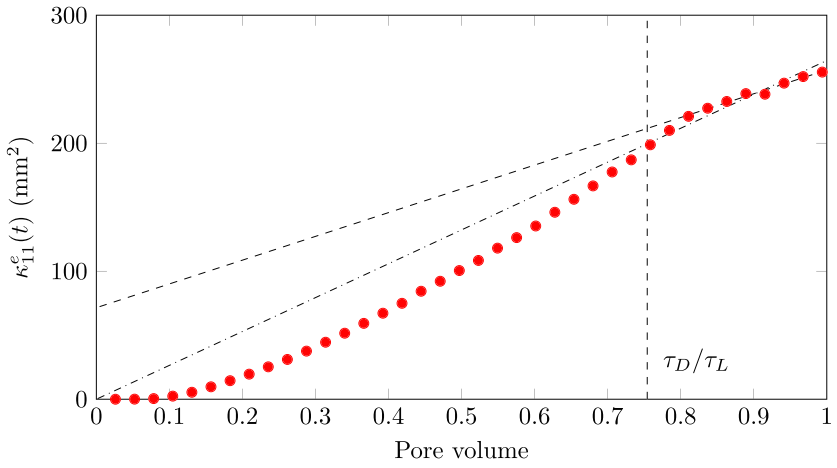

Figure 2. Evolution of $\kappa^e_{11}(t)$. The red symbols denote the data obtained from the experimental concentration distribution using 24, the dashed black line denotes the linear fit 29 for $t > \tau_D$, and the dash-dotted line represents the linear fit 30.

This has also been observed in other reactive transport experiments and simulations (de Anna, Dentz, et al., 2014; de Anna, Jiménez-Martínez, et al., 2014; Jose & Cirpka, 2004; Perez et al., 2019).

These mechanisms are reflected in the evolution of the total product mass shown in Figure 4. The strong nonlinear increase of the width of the mixing interface during early and intermediate times observed in Figure 2 produces fast growth in the production of C. This early-time growth is well captured by the dispersive lamella approach as shown in the inset of Figure 4. At increasing times, diffusive mixing reduces velocity contrast along the interface, and the growth rate of the mixing interface, and thus the production rate, slows down. These dynamics are well captured by the dispersive lamella approach. The dashed line in Figure 4 shows the mass production predicted by equation 10 for Fickian transport in an equivalent homogeneous medium characterized by porosity ϕ and the constant effective dispersion coefficient D^*. The characteristic $t^{1/2}$ scaling overestimates reactive mixing at short times because it overestimates the homogeneity of the interface. At intermediate and large times, it underestimates reactive mixing because it does not capture the nonlinear increase of the mixing interface due to advective heterogeneity; this means the transport and deformation history of the the mixing interface. The prediction based on the apparent hydrodynamic dispersion coefficient overestimates the mass because it simulates a homogeneity of the interface that does not

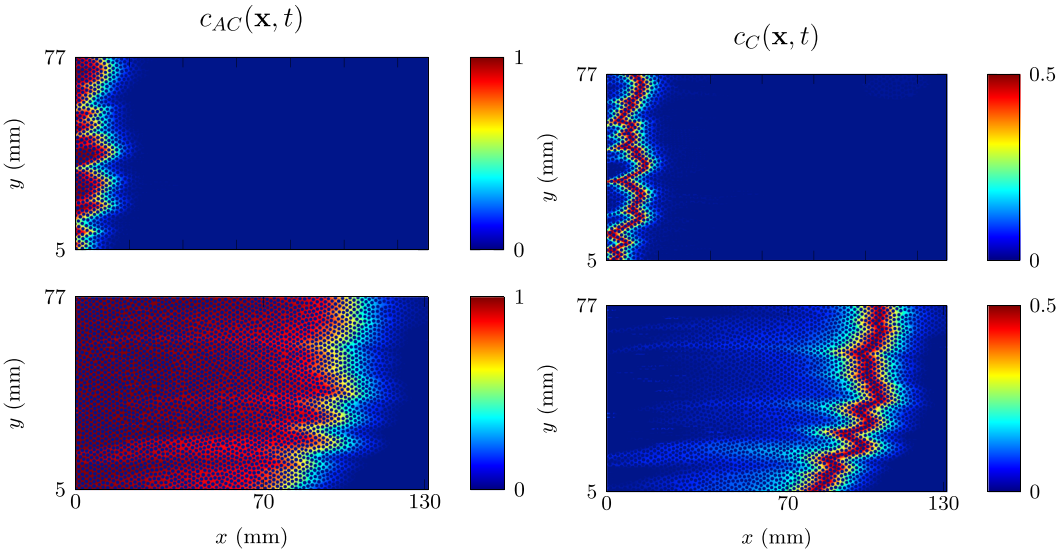

Figure 3. Concentration maps of the conservative component $c_{AC}(\mathbf{x}, t)$ (left) and the product concentration $c_C(\mathbf{x}, t)$ (right) at times (top to bottom) $t = 0.12$ and 0.77 pore volume.

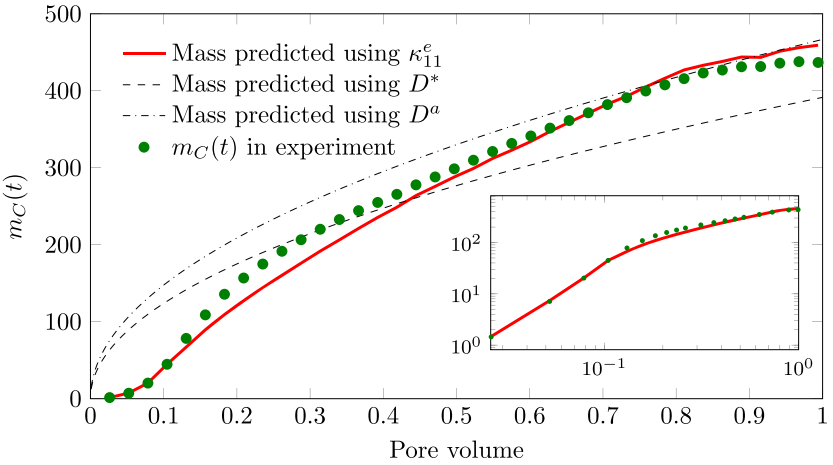

Figure 4. Evolution of $m_C(t)$ from the experimental visualization (green symbols), and predictions from the dispersive lamella (23) parameterized by $\kappa^e_{11}(t)$ (red line). The dashed line corresponds to the analytical prediction (10) based on D^*, and the dash-dotted line the prediction based on D^a. The inset graph in log-log axes is consistent with the legend and axis labels.

exist until asymptotic times when the support scale is well mixed. However, its definition 30 enforces that it coincides with the prediction of the lamellar approach at the time t_m. The dispersive lamella provides a systematic physics-based approach to quantify the impact of pore-scale mixing on Darcy scale reactive transport. It does not invoke additional reaction parameters but captures the dominant controls of the evolution of the mixing interface, namely, flow deformation and transverse mixing, in terms of an effective dispersion coefficient.

4. Conclusions

We study the impact of pore structure and flow heterogeneity on reactive mixing using data from an inert fluid-fluid displacement experiment in a quasi 2-D porous medium. The conservative concentration data is mapped onto the species concentrations for the fast irreversible reaction $A + B \rightarrow C$ using conservative components. This proposed methodology is valid if all reacting species have the same diffusion coefficients and in the absence of sorption and mass transfer between mobile and immobile regions.

The reaction efficiency is measured by the evolution of the total product mass, which for Fickian mixing increases as $t^{1/2}$. We observe a strong nonlinear increase of the product mass at short and intermediate times due to the combined action of advective heterogeneity, which causes deformation of the interface, and transverse mixing. Only at late times, when heterogeneity-induced mixing has homogenized the support scale, the reaction behavior may be captured in terms of constant hydrodynamic dispersion coefficients. For the experimental setup under consideration here, the effective longitudinal dispersion coefficient becomes asymptotic after about 10 cm. For more complex porous media, the corresponding time and space scales may be significantly larger.

The full global reaction behavior is quantified by a dispersive lamella approach. This approach represents the mixing interface through the superposition of Green functions of the pore-scale advection-diffusion problem; this means the concentration distribution evolving from a point injection. The Green functions are approximated by Gaussian distributions, termed dispersive lamellae, whose widths are characterized by effective dispersion coefficients. This terminology is motivated by stretched lamella approaches, which approximate the transport Green function using linear approximations of the flow velocity around the position of an advectively moving material element. Unlike the stretched lamella approach, the dispersive lamella accounts for the impact of transverse diffusion on the vertical homogenization of the mixing interface in terms of the effective dispersion coefficient. This approach upscales and predicts the reaction behavior based on pore-scale hydrodynamic fluctuations and diffusive mixing. It is predictive in the sense that it quantifies Darcy scale reaction behavior based only on effective dispersion coefficients, which quantify the dynamics of pore-scale heterogeneity-induced mixing. Thus, it provides a physics-based framework for the upscaling of mixing-limited reactions.

In this work, effective dispersion is estimated directly from the experimental data. Thus, the evolution of κ_{11}^{e} is not predicted but obtained from a conservative tracer test. While a large body of work exists in the literature for the derivation of constant hydrodynamic dispersion coefficients (Brenner & Edwards, 1993), we have not found any works on pore-scale effective dispersion. In general, however, it could be assessed by upscaling techniques based volume or stochastic averaging, for example, analogous to similar studies on the Darcy scale, which also capture the flowrate dependence of hydrodynamic dispersion. In conclusion, the proposed upscaled model provides a systematic and practical way for the prediction of non-Fickian mixing and reaction kinetics in heterogenous porous media.

Data Availability Statement

Data archiving is underway in the institutional open access repository DIGITAL.CSIC (digital.csic.es), where the data will be available with a unique and permanent document identifier.

Acknowledgments
We thank Olaf Cirpka, Nick Engdahl, and an anonymous reviewer for insightful and constructive comments. We acknowledge the support of the European Research Council (ERC) through the project MHetScale (617511) and the Spanish Ministry of Science and Innovation through a Severo-Ochoa Excellence Center Project (CEX2018-000794-S). JH acknowledges the support of the Spanish Ministry of Innovation and Universities through the Ramón y Cajal Program (RYC-2017-22300).

References

Bandopadhyay, A., Le Borgne, T., Méheust, Y., & Dentz, M. (2017). Enhanced reaction kinetics and reactive mixing scale dynamics in mixing fronts under shear flow for arbitrary Damköhler numbers. *Advances in Water Resources*, *100*, 78–95.

Battiato, I., & Tartakovsky, D. (2011). Applicability regimes for macroscopic models of reactive transport in porous media. *Journal of Contaminant Hydrology*, *120*, 18–26.

Battiato, I., Tartakovsky, D. M., Tartakovsky, A. M., & Scheibe, T. (2009). On breakdown of macroscopic models of mixing-controlled heterogeneous reactions in porous media. *Advances in Water Resources*, *32*(11), 1664–1673.

Beaudoin, A., de Dreuzy, J.-R., & Erhel, J. (2010). Numerical Monte Carlo analysis of the influence of pore-scale dispersion on macrodispersion in 2-D heterogeneous porous media. *Water Resources Research*, *46*, W12537. https://doi.org/10.1029/2010WR009576

Brenner, H., & Edwards, D. (1993). Macrotransport processes. Butterworth-Heinemann, MA, USA.

Cirpka, O. A. (2002). Choice of dispersion coefficients in reactive transport calculations on smoothed fields. *Journal Of Contaminant Hydrology*, *58*(3-4), 261–282.

Cirpka, O. A., & Kitanidis, P. K. (2000). An advective-dispersive stream tube approach for the transfer of conservative-tracer data to reactive transport. *Water Resources Research*, *36*(5), 1209–1220. https://doi.org/10.1029/1999WR900355

Danckwerts, P. (1952). The definition and measurement of some characteristics of mixtures. *Applied Scientific Research Section A*, *3*(4), 279–296.

Davis, J., Kent, D., Coston, J., Hess, K., & Joye, J. (2000). Multispecies reactive tracer test in an aquifer with spatially variable chemical conditions. *Water Resources Research*, *36*(1), 119–134. https://doi.org/10.1029/1999WR900282

de Anna, P., Dentz, M., Tartakovsky, A., & Le Borgne, T. (2014). The filamentary structure of mixing fronts and its control on reaction kinetics in porous media flows. *Geophysical Research Letters*, 41, 4586–4593. https://doi.org/10.1002/2014GL060068

de Anna, P., Jiménez-Martínez, J., Tabuteau, H., Turuban, R., Borgne, T. L., Derrien, M., & Méheust, Y. (2014). Mixing and reaction kinetics in porous media: An experimental pore scale quantification. *Environmental Science & Technology*, *48*(1), 508–516. https://doi.org/10.1021/es403105b

Dentz, M., Borgne, T. L., Englert, A., & Bijeljic, B. (2011). Mixing, spreading and reaction in heterogeneous media: A brief review. *Journal of Contaminant Hydrology*, *120-121*, 1–17. https://doi.org/10.1016/j.jconhyd.2010.05.002

Dentz, M., Kinzelbach, H., Attinger, S., & Kinzelbach, W. (2000). Temporal behavior of a solute cloud in a heterogeneous porous medium. 1. Point-like injection. *Water Resources Research*, *36*(12), 3591–3604. https://doi.org/10.1029/2000WR900162

Ding, D., Benson, D. A., Paster, A., & Bolster, D. (2013). Modeling bimolecular reactions and transport in porous media via particle tracking. *Advances in Water Resources*, *53*, 56–65. https://doi.org/10.1016/j.advwatres.2012.11.001

Edery, Y., Scher, H., & Berkowitz, B. (2010). Particle tracking model of bimolecular reactive transport in porous media. *Water Resources Research*, *46*, W07524. https://doi.org/10.1029/2009WR009017

Fendorf, S., Jardine, P. M., Patterson, R. R., Taylor, D. L., & Brooks, S. C. (1999). Pyrolusite surface transformations measured in real-time during the reactive transport of Co (II) EDTA2. *Geochimica et Cosmochimica Acta*, *63*(19-20), 3049–3057.

Fitts, C. R. (2002). *Groundwater science*: Elsevier.

Ginn, T. (2018). Modeling bimolecular reactive transport with mixing-limitation: Theory and application to column experiments. *Water Resources Research*, *54*, 256–270. https://doi.org/10.1002/2017WR022120

Gramling, C. M., Harvey, C. F., & Meigs, L. C. (2002). Reactive transport in porous media: A comparison of model prediction with laboratory visualization. *Environmental Science & Technology*, *36*(11), 2508–2514. https://doi.org/10.1021/es0157144

Gutierrez-Neri, M., Ham, P., Schotting, R., & Lerner, D. (2009). Analytical modelling of fringe and core biodegradation in groundwater plumes. *Journal of contaminant hydrology*, *107*(1-2), 1–9.

Hess, K. M., Davis, J. A., Kent, D. B., & Coston, J. A. (2002). Multispecies reactive tracer test in an aquifer with spatially variable chemical conditions, Cape Cod, Massachusetts: Dispersive transport of bromide and nickel. *Water Resources Research*, *38*(8), 1161. https://doi.org/10.1029/2001WR000945

Jiménez-Martinéz, J., de Anna, P., Tabuteau, H., Turuban, R., Borgne, T. L., & Méheust, Y. (2015). Pore-scale mechanisms for the enhancement of mixing in unsaturated porous media and implications for chemical reactions. *Geophysical Research Letters*, *42*, 5316–5324. https://doi.org/10.1002/2015GL064513

Jose, S. C., & Cirpka, O. A. (2004). Measurement of mixing-controlled reactive transport in homogeneous porous media and its prediction from conservative tracer test data. *Environmental Science & Technology*, *38*(7), 2089–2096.

Kapoor, V., Jafvert, C. T., & Lyn, D. A. (1998). Experimental study of a bimolecular reaction in Poiseuille flow. *Water Resources Research*, *34*(8), 1997–2004.

Kitanidis, P. K. (1988). Prediction by the method of moments of transport in a heterogeneous formation. *Journal of Hydrology*, *102*(1-4), 453–473.

Kitanidis, P. K. (1994). The concept of the dilution index. *Water Resources Research*, *30*(7), 2011–2026. https://doi.org/10.1029/94wr00762

Le Borgne, T., Dentz, M., & Villermaux, E. (2015). The lamellar description of mixing in porous media. *Journal of Fluid Mechanics*, *770*, 458–498.

Le Borgne, T., Ginn, T. R., & Dentz, M. (2014). Impact of fluid deformation on mixing-induced chemical reactions in heterogeneous flows. *Geophysical Research Letters*, *41*, 7898–7906. https://doi.org/10.1002/2014GL062038

Li, L., Peters, C. A., & Celia, M. A. (2006). Upscaling geochemical reaction rates using pore-scale network modeling. *Advances in Water Resources*, *29*(9), 1351–1370. https://doi.org/10.1016/j.advwatres.2005.10.011

Matlock, M. M., Howerton, B. S., & Atwood, D. A. (2001). Irreversible precipitation of mercury and lead. *Journal of Hazardous Materials*, *84*(1), 73–82.

Oates, P. M., & Harvey, C. F. (2006). A colorimetric reaction to quantify fluid mixing. *Experiments in Fluids*, *41*(5), 673–683.

Perez, L. J., Hidalgo, J. J., & Dentz, M. (2019). Upscaling of mixing-limited bimolecular chemical reactions in Poiseuille flow. *Water Resources Research*, *55*, 249–269. https://doi.org/10.1029/2018WR022730

Raje, D. S., & Kapoor, V. (2000). Experimental study of bimolecular reaction kinetics in porous media. *Environmental Science & Technology*, *34*(7), 1234–1239.

Ranz, W. E. (1979). Applications of a stretch model to mixing, diffusion, and reaction in laminar and turbulent flows. *AIChE Journal*, *25*(1), 41–47.

Rolle, M., Chiogna, G., Hochstetler, D. L., & Kitanidis, P. K. (2013). On the importance of diffusion and compound-specific mixing for groundwater transport: An investigation from pore to field scale. *Journal of contaminant hydrology*, *153*, 51–68.

Rolle, M., Eberhardt, C., Chiogna, G., Cirpka, O. A., & Grathwohl, P. (2009). Enhancement of dilution and transverse reactive mixing in porous media: Experiments and model-based interpretation. *Journal of Contaminant Hydrology*, *110*(3), 130–142.

Sanchez-Vila, X., Fernández-Garcia, D., & Guadagnini, A. (2010). Interpretation of column experiments of transport of solutes undergoing an irreversible bimolecular reaction using a continuum approximation. *Water Resources Research*, *46*, W12510. https://doi.org/10.1029/2010WR009539

Savitzky, A., & Golay, M. J. (1964). Smoothing and differentiation of data by simplified least squares procedures. *Analytical Chemistry*, *36*(8), 1627–1639.

Simoni, M. D., Carrera, J., Sánchez-Vila, X., & Guadagnini, A. (2005). A procedure for the solution of multicomponent reactive transport problems. *Water Resources Research*, *41*, W11410. https://doi.org/10.1029/2005WR004056

Steefel, C., Depaolo, D., & Lichtner, P. (2005). Reactive transport modeling: An essential tool and a new research approach for the Earth sciences. *Earth and Planetary Science Letters*, *240*(3-4), 539–558. https://doi.org/10.1016/j.epsl.2005.09.017

Tartakovsky, A., Tartakovsky, G., & Scheibe, T. (2009). Effects of incomplete mixing on multicomponent reactive transport. *Advances in Water Resources*, *32*, 1674–1679. https://doi.org/10.1016/j.advwatres.2009.08.012

Valocchi, A. J., Bolster, D., & Werth, C. J. (2019). Mixing-limited reactions in porous media. *Transport in Porous Media*, *130*(1), 157–182.

Willingham, T. W., Werth, C. J., & Valocchi, A. J. (2008). Evaluation of the effects of porous media structure on mixing-controlled reactions using pore-scale modeling and micromodel experiments. *Environmental Science & Technology*, *42*(9), 3185–3193. https://doi.org/10.1021/es7022835